SUBMITTED TO APJ JANUARY 4, 2007
Preprint typeset using LaTeX style emulateapj v. 11/26/04

THE TEV SOURCE HESS J1804–216 IN X-RAYS AND OTHER WAVELENGTHS

O. KARGALTSEV, G. G. PAVLOV, AND G. P. GARMIRE
The Pennsylvania State University, 525 Davey Lab, University Park, PA 16802, USA
Submitted to ApJ January 4, 2007

ABSTRACT

The field of the extended TeV source HESS J1804–216 was serendipitously observed with the *Chandra* ACIS detector on 2005 May 4. The data reveal several X-ray sources within the bright part of HESS J1804–216. The brightest of these objects, CXOU J180432.4–214009, which has been also detected with *Swift* (2005 November 3) and *Suzaku* (2006 April 6), is consistent with being a point-like source, with the 0.3–7 keV flux $F_X = (1.7 \pm 0.2) \times 10^{-13}$ ergs s^{-1} cm^{-2}. Its hard and strongly absorbed spectrum can be fitted by the absorbed power-law model with the best-fit photon index $\Gamma \approx 0.45$ and hydrogen column density $n_{\rm H} \approx 4 \times 10^{22}$ cm^{-2}, both with large uncertainties due to the strong correlation between these parameters. A search for pulsations resulted in a 106 s period candidate, which however has a low significance of 97.9%. We found no infrared-optical counterparts for this source. The second brightest source, CXOU J180441.9–214224, which has been detected with *Suzaku*, is either extended or multiple, with the flux $F_X \sim 1 \times 10^{-13}$ ergs cm^{-2} s^{-1}. We found a nearby M dwarf within the X-ray source extension, which could contribute a fraction of the observed X-ray flux. The remaining sources are very faint ($F_X < 3 \times 10^{-14}$ ergs cm^{-2} s^{-1}), and at least some of them are likely associated with nearby stars. Although one or both of the two brighter X-ray sources could be faint accreting binaries or remote pulsars with pulsar wind nebulae (hence possible TeV sources), their relation to HESS J1804–216 remains elusive. The possibility that HESS J1804–216 is powered by the relativistic wind from the young pulsar B1800–21, located at a distance of ~ 10 pc from the TeV source, still remains a more plausible option.

Subject headings: X-rays: individual (CXOU J180432.4–214009, CXOU J180441.9–214224, HESS J1804–216) — pulsars: individual (PSR B1800–21=J1803–2137)

1. INTRODUCTION

Recent observations with the High Energy Stereoscopic System (HESS) and other modern very high energy (VHE) telescopes have revealed a rich population of TeV γ-ray sources (Aharonian et al. 2005). A significant fraction of these sources are associated with various types of known astrophysical phenomena (see Ong 2006 for a review). The list of Galactic TeV sources with firm associations includes high mass X-ray binaries (HMXBs), supernova remnants (SNRs), and pulsar wind nebulae (PWNe). Extragalactic TeV sources are so far represented only by AGNs (mostly blazars). Many of the newly discovered TeV sources are extended and resolved in the HESS images. Most of the identified extended sources are PWNe and SNRs, although there is an indication that some HMXBs could also produce extended TeV emission (e.g., HESS J1632–478; Aharonian et al. 2006a, hereafter Ah06). Among the known Galactic TeV sources, only HMXBs are variable in TeV, some of them showing variations with the binary orbital period (e.g., the microquasar LS 5039, Aharonian et al. 2006b). The extragalactic AGN sources appear to be point-like at TeV energies and can also be variable.

A quarter of the ≈ 50 VHE sources known to date[1] do not have firm identifications, although possible counterparts/associations have been suggested for some of them. HESS J1804–216 (hereafter HESS J1804), the brightest among such sources, has been recently discovered during the HESS Galactic plane scan in 2004 May–October (Aharonian et al. 2005). The "best-fit position" of the source (which is close to, but may be different from, the peak in the TeV brightness distribution; see Ah06 for definition) is R.A.=$18^{\rm h}04^{\rm m}31^{\rm s}$, Decl.=–21°42′.0, with a 1′.3 uncertainty in each of the coordinates. The distribution of the TeV brightness shows an extended source with elongated morphology (see the contours in Fig. 17 of Ah06). The size of the source, $\gtrsim 20' \times 10'$, substantially exceeds the size of the HESS point spread function (PSF), $\approx 6'$ for this observation (Ah06). The large extent of the TeV emission rules out its association with an AGN, which means that HESS J1804 is a Galactic source.

Ah06 point out that the TeV emission does not perfectly line up with any known sources in the field. Among possible counterparts, Ah06 mention the young Vela-like pulsar B1800–21 and the SNR G8.7–0.1, both of which have been detected in X-rays (Kargaltsev, Pavlov, & Garmire 2006a and Finley & Ögelman 1994, respectively). Ah06 also do not dismiss the possibility that HESS J1804 and other unidentified TeV sources belong to a new class of objects sometimes dubbed "dark particle accelerators" (Aharonian et al. 2005a) because of the apparent lack of counterparts outside the TeV band.

Following the discovery of HESS J1804, the field was observed in X-rays by the *Swift* X-ray Telescope (XRT) instrument on 2005 November 3 (Landi et al. 2006) and *Suzaku* X-ray Imaging Spectrometers (XIS) on 2006 April 6 (Bamba et al. 2006). Landi et al. (2006) detected three X-ray sources in the 23′.6 × 23′.6 *Swift* XRT detector field-of-view (FOV), at distances of 13′.3, 7′.4, and 2′.0 (positional uncertainty $\sim 5''$–$6''$) from the best-fit HESS position (we will call them Sw1, Sw2, and Sw3 hereafter). Sw1 and Sw2 had been previously detected with *ROSAT*. Sw1 (= 1RXS J180404.6–215325), the brightest of the 3 sources, shows a very soft thermal-like spectrum ($kT \approx 0.3$ keV for an optically thin thermal bremsstrahlung model), and it is positionally coincident with

Electronic address: pavlov@astro.psu.edu
[1] See the catalogs at http://www.icrr.u-tokyo.ac.jp/m̃orim/TeV-catalog.htm and http://www.mpi-hd.mpg.de/hfm/HESS/public/HESS_catalog.htm

a bright star outside the extension of the TeV source. The spectra of Sw2 (= 1WGA J1804.0-2142) and Sw3 could not be measured because of the small numbers of counts detected (22 ± 7 and 26 ± 6 counts, respectively, in the 11.6 ks exposure). Sw2 could also be associated with a star close to the boundary of the XRT error circle, while Sw3, closest to the center of HESS J1804, did not show obvious counterparts at other wavelengths.

The subsequent deeper (40 ks) *Suzaku* XIS observation revealed two distinct X-ray sources (Suzaku J1804–2142 and Suzaku J1804–2140; Su42 and Su40 hereafter) in the $18' \times 18'$ XIS FOV. Su40 is positionally coincident with Sw3 within the large ($\sim 1'$) positional uncertainty of *Suzaku* XIS. Bamba et al. (2006) found that Su40 is extended (or multiple) while Su42 is unresolved at the *Suzaku* resolution (half power PSF diameter $\approx 2'$). Spectral fits with a power-law (PL) model show markedly different spectral parameters for the two sources. Su42 was found to be unusually hard (photon index $\Gamma = -0.3^{+0.5}_{-0.5}$, the errors are at the 90% confidence for one interesting parameter) with a moderate (albeit rather uncertain) hydrogen column density, $n_{\rm H,22} \equiv n_{\rm H}/(10^{22}\,{\rm cm}^{-2}) = 0.2^{+2.0}_{-0.2}$. Su40 showed a softer ($\Gamma = 1.7^{+1.4}_{-1.0}$), strongly absorbed ($n_{\rm H,22} = 11^{+10}_{-6}$) spectrum. The sources have comparable fluxes, ~ 2.5 and 4.3×10^{-13} ergs cm^{-2} s^{-1} in 2–10 keV, for Su42 and Su40, respectively. Despite an appreciable probability of chance coincidence (obvious from the *Chandra* images in §2), Bamba et al. (2006) conclude that both *Suzaku* sources are physically associated with HESS J1804. They mention that the harder Su42 could be an HMXB while the softer Su40 could be either a PWN or, more likely, it could be associated with SNR G8.7–0.1. The authors also point out that the ratios of the γ-ray flux of HESS J1804 to the X-ray fluxes of Su42 and Su40 are surprisingly high compared to those seen in TeV sources with known associations, including SNRs and PWNe. Thus, the *Swift* and *Suzaku* data do not provide a conclusive result on the nature of HESS J1804, and its association with the found X-ray sources remains unclear.

In the course of our observation of PSR B1800–21 and its PWN with the *Chandra X-ray Observatory*, the most interesting part of the HESS J1804 field happened to be within the FOV. Detailed results of the PWN/PSR B1800–21 study have been presented by Kargaltsev et al. (2006a). In this paper we present the analysis of X-ray sources in the vicinity of HESS J1804, including the two sources detected with *Suzaku*[2]. The details of the *Chandra* observation and the data analysis, supplemented with the analysis of optical-infrared-radio data, are presented in §2. We discuss the nature of the *Chandra* sources and the likelihood of their association with HESS J1804 in §3, and summarize our findings in §4.

2. OBSERVATIONS AND DATA ANALYSIS

We serendipitously observed the field of HESS J1804 with the Advanced CCD Imaging Spectrometer (ACIS) on board *Chandra* on 2005 May 4. The total useful scientific exposure time was 30,236 s. The observation was carried out in Faint mode. The aim point was chosen on S3 chip, near the PSR B1800–21 position (see Kargaltsev et al. 2006a). In addition to S3, the S0, S1, S2, I2, and I3 chips were turned on. The detector was operated in Full Frame mode which provided time resolution of 3.24 seconds. The data were reduced using the Chandra Interactive Analysis of Observations (CIAO) software (ver. 3.2.1; CALDB ver. 3.0.3).

[2] It should be noted that after this paper had been generally completed, Cui & Konopelko (2006) published an ApJ letter using the same *Chandra* data. Using wrong coordinates of PSR B1800–21, they could not identify the pulsar in the *Chandra* image, failed to notice one of the two *Suzaku* sources, and did not provide a thorough analysis of the other Suzaku source. We correct the shortcomings of that work in our paper.

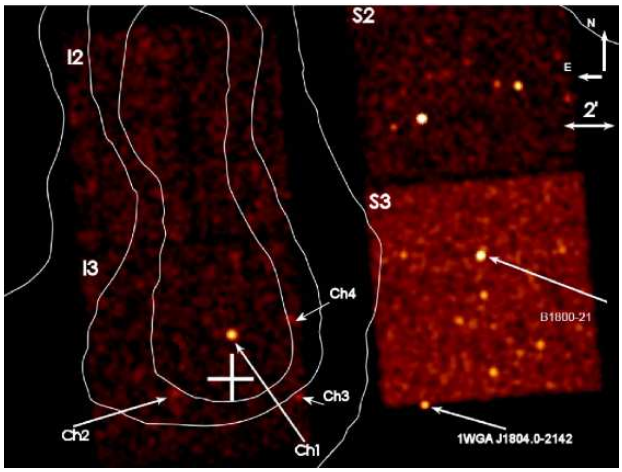

FIG. 1.— *Chandra* ACIS image (0.5–8 keV; smoothed with a $r = 6''$ gaussian kernel) of the central part of HESS J1804 with the TeV contours overlayed. The best-fit position of HESS J1804 and its uncertainty are marked by the cross. The arrows show the four brightest X-ray sources, Ch1 (CXOU J180432.4–214009 = Sw3 = Su40), Ch2 (CXOU 180441.9–214224 = Su42), Ch3 (CXOU J180421.5–214233), and Ch4 (CXOU J180423.1–213932), detected in the brighter part of the TeV image, the pulsar B1800–21, and the *ROSAT* source 1WGA 1804.0–2142 (= Sw2). (Sw1, the brightest of the sources detected with *Swift*, is out of the ACIS FOV: it is shown in the *ROSAT* image in Fig. 8.)

2.1. *Chandra images*

Figure 1 shows the ACIS image of the HESS J1804 field with overlaid TeV contours, extracted from Figure 17 of Ah06. The brightest portion of HESS J1804 falls onto the I3 and I2 chips, its best-fit position is offset by $\approx 11.'2$ from the aim point. We searched for possible X-ray counterparts within the HESS J1804 extension and found a relatively bright source, which we designate CXOU J180432.4–214009 (hereafter Ch1), located at R.A. = $18^{\rm h}04^{\rm m}32.^{\rm s}462$, decl. = $-21^\circ 40' 09.''91$ (the 1σ centroid uncertainty is $0.''38$ in R.A. and $0.''32$ in decl.; the 1σ error in absolute *Chandra* astrometry is $\approx 0.''4$ for each of the coordinates), well within the brightest portion of HESS J1804 and just $1.'9$ north of the best-fit position (Ah06). Although Ch1 appears to be slightly extended in the ACIS image, a PSF simulation shows that this is likely the result of the off-axis location (off-axis angle $\theta = 10.'3$), which is also responsible for the relatively large centroiding uncertainty quoted above. The position of Ch1 is consistent (within the uncertainties) with that of Sw3 and Su40 (see §1). Therefore, we conclude that Ch1, Sw3, and Su40 represent the same source, although we found no evidence of the $\sim 2'$–$3'$ extension reported by Bamba et al. (2006) for Su40.

We barely see some excess counts within the Su42 error circle in the original ACIS image, scattered over an area exceeding the PSF even with account for the large off-axis angle, $\theta \approx 14'$. However, when we filter out photons with energies > 8 keV (which effectively reduces the background by a factor of 2.7) and bin by a factor of 8 (i.e., the new pixel size is $3.''9$), an extended (or multiple) source becomes visible, with a size of $\simeq 1.'5 - 2'$ (see Fig. 2). The best-fit centroid of the source (obtained with the CIAO *wavdetect* tool) is R.A. = $18^{\rm h}04^{\rm m}41.^{\rm s}924$, Decl.= $-21^\circ 42' 24.''09$; we designate the source as CXOU J180441.9–214224 (hereafter Ch2).

In addition to Ch1 and Ch2, we found a dozen

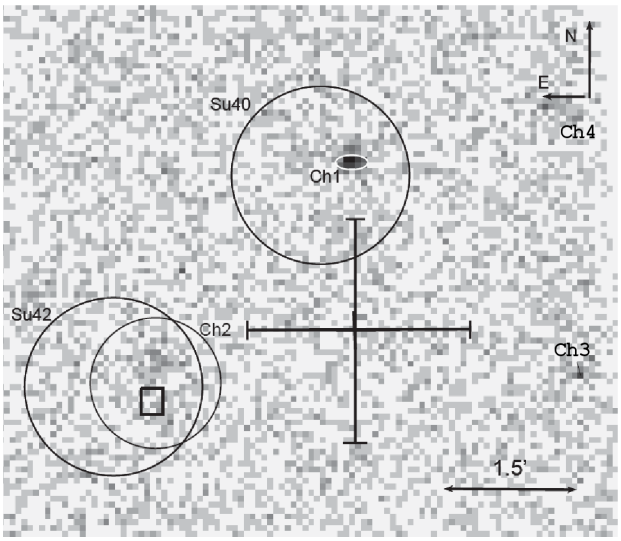

FIG. 2.— *Chandra* ACIS-I3 image (in the 0.5–8 keV band; binned by a factor of 8) of the HESS J1804 central region. The best-fit position of HESS J1804 from Ah06 is shown by the cross. The position of the M-type dwarf (see §2.4) is shown by the box. Two larger circles ($r = 1'$) are centered at the positions of Su40 and Su42 as reported by Bamba et al. (2006). The smaller circle ($r = 44''$) shows the region used to estimate the count rates from Ch2 while the small ellipse shows the region used for the Ch1 spectral extraction. An offset of about $15''$ between the positions of the *Chandra* sources and *Suzaku* sources is apparently due to inaccuracy in *Suzaku* aspect solution. The fainter Ch3 and Ch4 sources (see text) are also marked.

fainter sources on the I3 and I2 chips, of which CXOU J180421.5−214233 and CXOU J180423.1−213932 (hereafter Ch3 and Ch4, respectively) are the brightest and the closest to the best-fit position of HESS J1809 (see Figs. 1 and 2). Ch3 is consistent with being point-like, while Ch4 is either extended or, more likely, multiple.

We also attempted to search for signatures of diffuse emission (e.g., an SNR) on the I3 chip. A direct visual inspection of the ACIS image did not show clear signatures of large-scale diffuse emission. We applied the exposure map correction and smoothed the image with various scales, but failed to find statistically significant deviations from a uniform brightness distribution. To estimate an upper limit on the SNR emission, we measured the count rate from the entire I3 chip (with all identifiable point sources removed). The count rate, 0.266 ± 0.003 counts s^{-1} in the 0.5–7 keV band, exceeds the nominal I3 background of 0.17 counts s^{-1} (*Chandra* Proposers' Observatory Guide[3], v.8, §6.15.2), which could be caused by an elevated particle background, diffuse X-ray background, or SNR emission. Since we see no clear evidence of an SNR, we consider the difference, ≈ 0.09 counts s^{-1}, as an upper limit on the SNR count rate in the 70 arcmin^2 of the chip area, which corresponds the average surface brightness limit of 1.3 counts ks^{-1} arcmin^{-2}.

2.2. *Spectral analysis of the Chandra sources*

We extracted the Ch1 spectrum from the elliptical region (with the minor and major axes of $4\farcs9$ and $10\farcs8$; see Fig. 2), which accounts for the elongated shape of the off-axis PSF and contains $\approx 83\%$ of the source counts. The background was measured from a larger circular annulus; it contributes about 15% to the total of 127 counts within the source extraction region. We group the spectra into 10 spectral bins between 0.3 and 7 keV. The spectrum of the source (shown in Fig. 3) is strongly absorbed, with only five counts below

[3] See http://asc.harvard.edu/proposer/POG/index.html

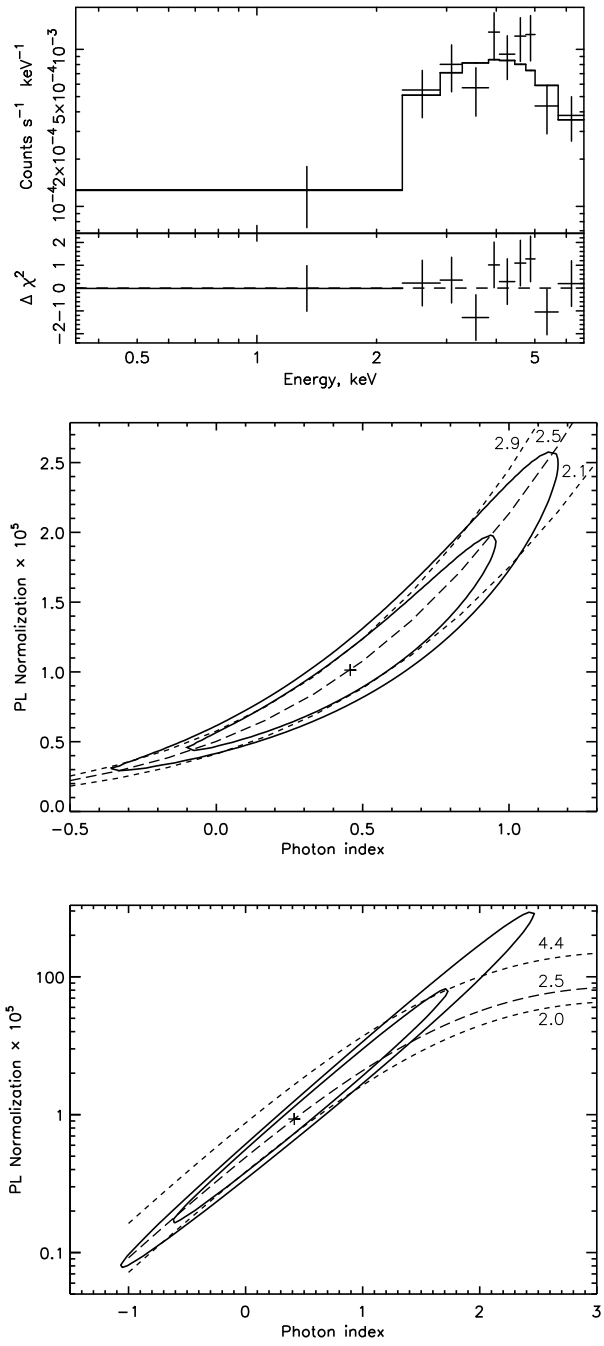

FIG. 3.— Ch1 spectrum fitted with the PL model (*top*) and the corresponding confidence contours (68% and 90%) obtained with the $n_{\rm H}$ held fixed at the best-fit value (*middle*) and n_H fitted at each grid point (*bottom*). The PL normalization (vertical axis) is in units of 10^{-5} photons cm^{-2} s^{-1} keV^{-1} at 1 keV. The lines of constant unabsorbed flux (in units of 10^{-13} ergs cm^{-2} s^{-1}; in 0.5–8 keV band) are plotted as dashed lines.

2 keV (the lowest photon energy is 0.35 keV). The absorbed PL model fits the spectrum well, $\chi^2_\nu = 0.99$ for 7 degrees of freedom, with $n_{\rm H,22} \approx 3.8$, $\Gamma \approx 0.45$, and the absorbed and unabsorbed fluxes of (1.7 ± 0.2) and $(2.5^{+0.9}_{-0.4}) \times 10^{-13}$ erg cm^{-2} s^{-1} in 0.3–7 and 0.3–8 keV, respectively. (Here and below the *Chandra* fluxes, luminosities and PL normalizations are corrected for vignetting and for the finite extraction aperture.) The uncertainties of the fits are listed in Table 1 and illustrated by confidence contours in Figures 3 and 4. As one can see, fixing the absorption at the best-fit value substantially reduces

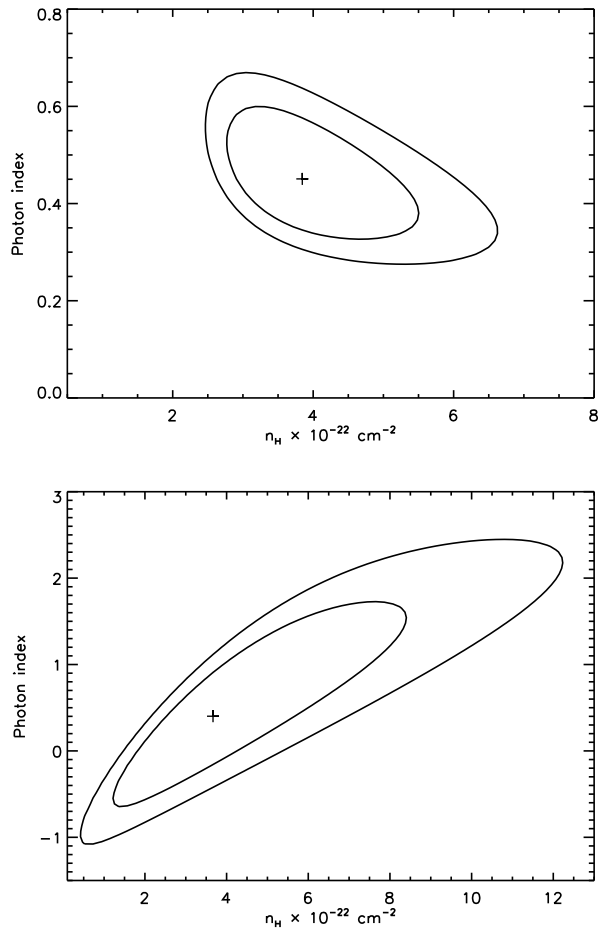

FIG. 4.— Confidence contours (68% and 90%) in the $n_{\rm H}$–Γ plane for the PL fit to the Ch1 spectrum. The *top* panel shows contours obtained with the PL normalization held fixed at the best-fit value (see Table 1) while in the *bottom* panel the PL normalization was fitted at each grid point in the Γ–n_H space.

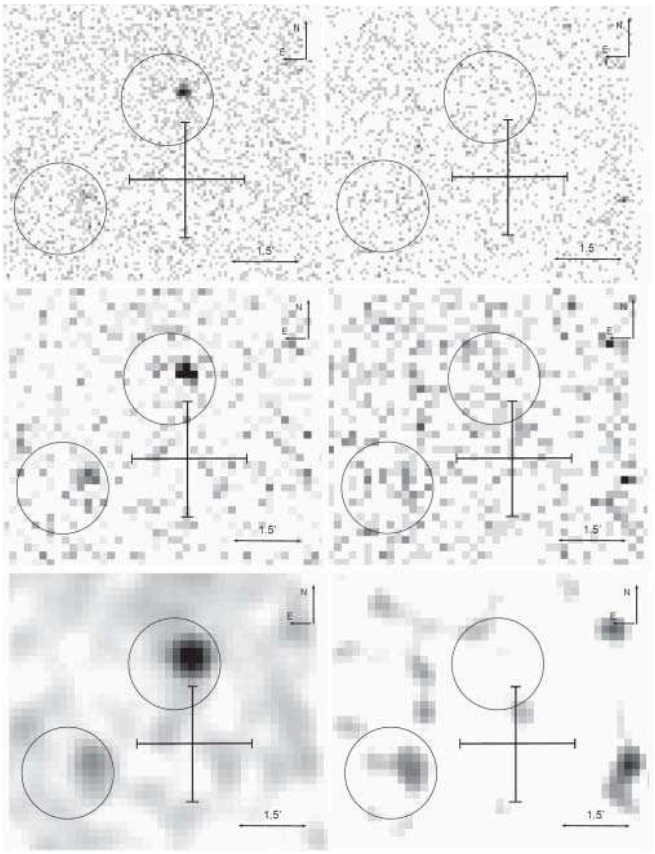

FIG. 5.— Hard (2–7 keV; *left*) and soft (0.5–2 keV; *right*) band *Chandra* images of the HESS J1804 central region. The best-fit position of HESS J1804 (Ah06) is shown by the cross. The circles ($r = 1'$) are centered at the positions of the two X-ray sources seen by *Suzaku* XIS (Bamba et al. 2006). The images in the *top* panels are binned by a factor of 8 (pixel size $3\farcs9$) while the same images in the *middle* panels are binned by a factor of 20 (pixel size $9\farcs8$). The *bottom* panels show the same images binned by a factor of 20 and smoothed with a $30''$ gaussian kernel.

the uncertainties of the remaining parameters since Γ and n_H are strongly correlated. At a fiducial distance of 8 kpc, the observed PL flux corresponds to the unabsorbed luminosity of $\sim 2\times10^{33}$ ergs s^{-1}. Even with account for the large uncertainties, the spectral parameters are in poor agreement with those obtained by Bamba et al. (2006) for Su40, although an accurate comparison is difficult because those authors do not provide confidence contours. The *Chandra* and *Suzaku* unabsorbed fluxes, which are more accurately measured than the spectral parameters, are consistent within their uncertainties: $3.3^{+1.2}_{-0.5}\times10^{-13}$ versus $4.3^{+4.0}_{-1.1}\times10^{-13}$ ergs s^{-1} cm^{-2} in the 2–10 keV band, respectively. The ACIS spectrum of Ch1 also fits an absorbed black-body (BB) model with the temperature of 2.3 keV and emitting region radius of $\sim 30(d/8\,{\rm kpc})$ m. The uncertainties of the BB fit are even larger than those of the PL fit.

For Ch2, the total number of background-subtracted counts within the $r = 44''$ aperture centered at the source position (see Fig. 2) is 73 ± 19 in 0.3–8 keV (the total number of counts is 307, of which 234 counts are estimated to come from the background). Restricting the photon energies to the hard, 2–7 keV, band results in a similar $S/N = 3.1$ (55 ± 12 net source counts), while $S/N = 2.1$ (28 ± 13 net source counts) in the soft, 0.5–2 keV, band. These numbers indicate a relatively hard spectrum of the source, in qualitative agreement with the Su42 spectrum as reported by Bamba et al. (2006). The hard and soft band images are shown in Figure 5. The low S/N values preclude a reliable spectral fitting. The measured count rates correspond to the observed 0.3–8 keV flux of $(1.0\pm0.3)\times10^{-13}$ ergs s^{-1} cm^{-2} in the $r = 44''$ aperture, and the unabsorbed flux of $\approx 1.5\times10^{-13}$ ergs s^{-1} cm^{-2} in 2–10 keV, using the best-fit spectral parameters reported by Bamba et al. (2006) for Su42. The estimated unabsorbed flux of Ch2 is a factor of ≈ 1.7 smaller than the flux of Su42, $(2.5\pm0.4)\times10^{-13}$ ergs s^{-1} cm^{-2} reported by Bamba et al. (2006); however, the difference may be due to unaccounted systematic errors.

For Ch3 and Ch4, the background-subtracted numbers of counts in the 0.5–8 keV band are 19 ± 5 and 44 ± 10, in $r = 7\farcs4$ and $21''$ apertures, respectively (we chose the larger aperture for Ch4 because it looks extended or multiple). Their observed fluxes can be crudely estimated as ~ 1.2 and $\sim 2.5\times10^{-14}$ ergs cm^{-2} s^{-1}, respectively. The low S/N does not allow a meaningful spectral analysis of these sources. Figure 5 shows, however, that both Ch3 and Ch4 are better seen in the soft band, which means that they are less absorbed (hence less distant) than Ch1 and Ch2. Since the other off-axis sources on I3 and I2 chips are even fainter, their flux estimates are not reliable.

2.3. *Timing of Ch1*

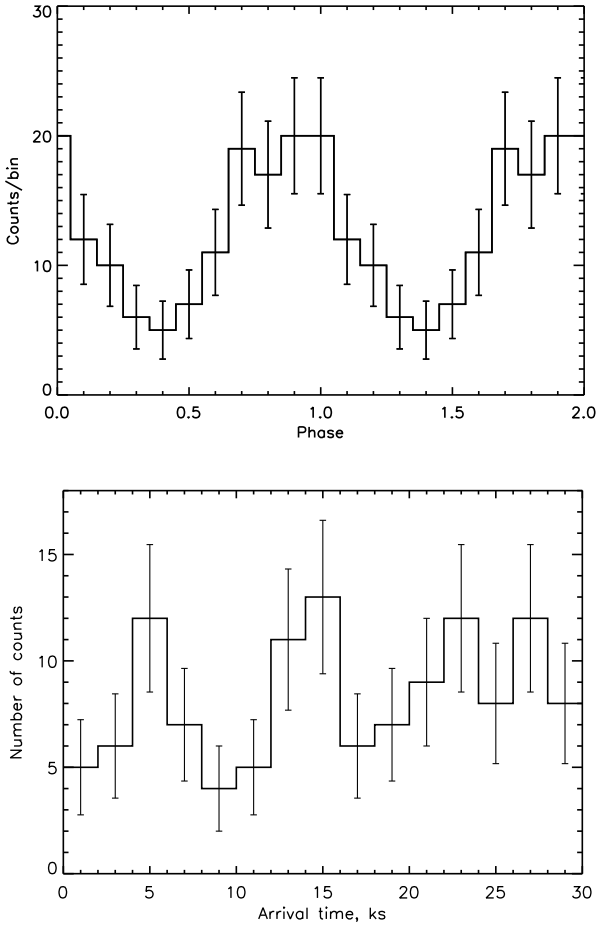

FIG. 6.— *Top:* Light curve of Ch1 folded with the period of 106.12 s. *Bottom:* Unfolded light curve of Ch1.

We searched for pulsations of Ch1, using the arrival times of the 127 photons (of which ≈ 85% on are expected to come from the source) recalculated to the solar system barycenter using the CIAO `axBary` tool. The ACIS time resolution of 3.24 s and the total time span of 30 ks allow a search for pulsations in a 3×10^{-5}–0.1 Hz range. We calculated the Z_1^2 statistic (e.g., Zavlin et al. 2000) at 10^5 equally spaced frequencies ν in the 3×10^{-5}–0.1 Hz range. This corresponds to oversampling by a factor of about 33, compared to the expected width of $T_{\rm span}^{-1}\approx 33$ μHz of the $Z_1^2(\nu)$ peaks, and guarantees that we miss no peaks. The most significant peak, $Z^2_{1,\rm max}=23.70$, was found at $\nu = 0.009423\,{\rm Hz}\pm5\,\mu{\rm Hz}$ ($P\approx106.12\pm0.05$ s). The maximum value of Z_1^2 corresponds to the 97.9% ($\approx2.3\sigma$) significance level, for the number of independent trials $\mathcal{N}=\nu_{\rm max}T_{\rm span}\approx3\times10^3$. The pulse profile folded with the above frequency is shown in Figure 6 (*top*). The corresponding observed pulsed fraction is $58\%\pm13\%$ (intrinsic source pulsed fraction $\approx67\%\pm15\%$) The significance of the period candidate is rather low, so the periodicity should be tested in a longer observation.

We also produced the unfolded light curve of Ch1 (Fig. 8, *bottom*) using a 2 ks binning. The light curve indicates that the source may experience some non-periodic variability on a few ks scale.

2.4. *Optical-IR-radio data*

TABLE 1
FITS TO THE SPECTRUM OF CH1

Model	$n_{\rm H,22}$	$\mathcal{N}$[a] or Area[b]	Γ or kT[c]	χ^2/dof	$L_{\rm X}$ or $L_{\rm bol}$[d]
PL	$3.8^{+4.2}_{-2.5}$	$10.2^{+200}_{-5.7}$	$0.45^{+2.05}_{-1.45}$	6.9/6	$1.9^{+0.7}_{-0.3}$
PL	3.8[e]	$10.2^{+3.6}_{-2.7}$	$0.45^{+0.34}_{-0.39}$	6.9/7	1.9 ± 0.2
BB	$2.6^{+1.8}_{-1.2}$	~2.9	~2.3	6.8/6	~7.9

NOTE. — The uncertainties are given at the 68% confidence level for one interesting parameter.
[a] Spectral flux in 10^{-6} photons cm^{-2} s^{-1} keV^{-1} at 1 keV
[b] Projected area of the emitting region for the BB model in 10^3 m^2 (assuming an 8 kpc distance).
[c] BB temperature in keV.
[d] Unabsorbed luminosity in 0.5–8 keV band or bolometric luminosity in units of 10^{33} erg s^{-1} at the distance of 8 kpc.
[e] The hydrogen column density was frozen at this value during the fit.

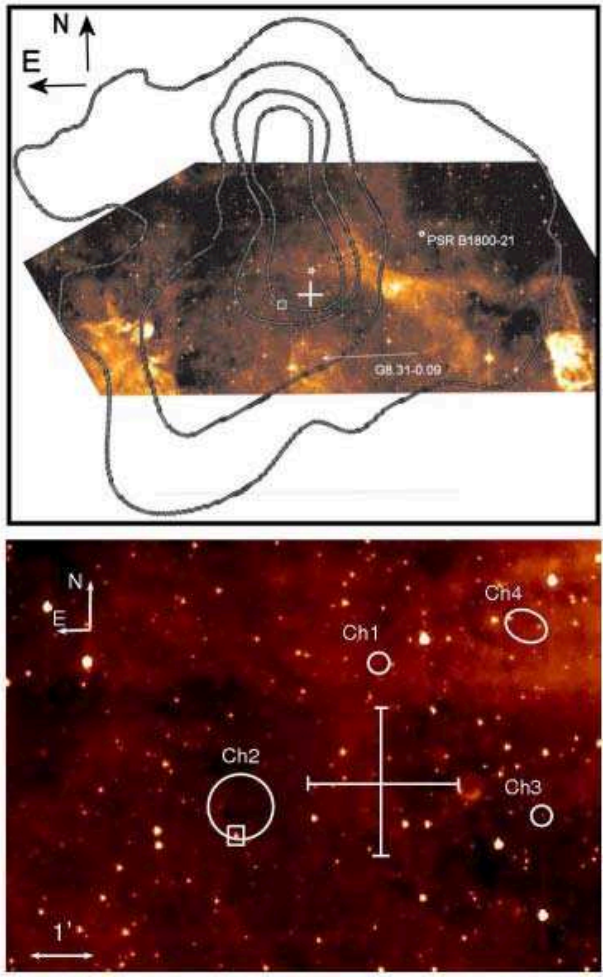

FIG. 7.— *Top:* 8 μm *Spitzer* IRAC image of the HESS J1804 field with TeV contours overlayed. The best-fit position of HESS J1804 is shown by the cross. The positions of Ch1 and Ch2 are marked with the star and box respectively. The position of PSR B1800–21 is marked with a diamond, and the possible new SNR G8.31–0.09 is shown by the arrow. *Bottom:* Blow-up of the central part of the image. The two $r = 10''$ circles, the larger $28''$ circle, and the $14''\times20''$ ellipse are centered at the positions of Ch1, Ch3, Ch2, and Ch4, respectively. The M dwarf near the Ch2 position is shown by the box.

We found no counterparts to Ch1 within $9''$ from its position in the Two Micron All Sky Survey (2MASS; Cutri et al. 2003) or Digital Sky Survey (DSS2)[4] catalogs up to the limiting magnitudes $K_s = 15.4$, $H = 16$, $J = 17.5$, $R = 19$, and

[4] see http://archive.eso.org/dss/dss

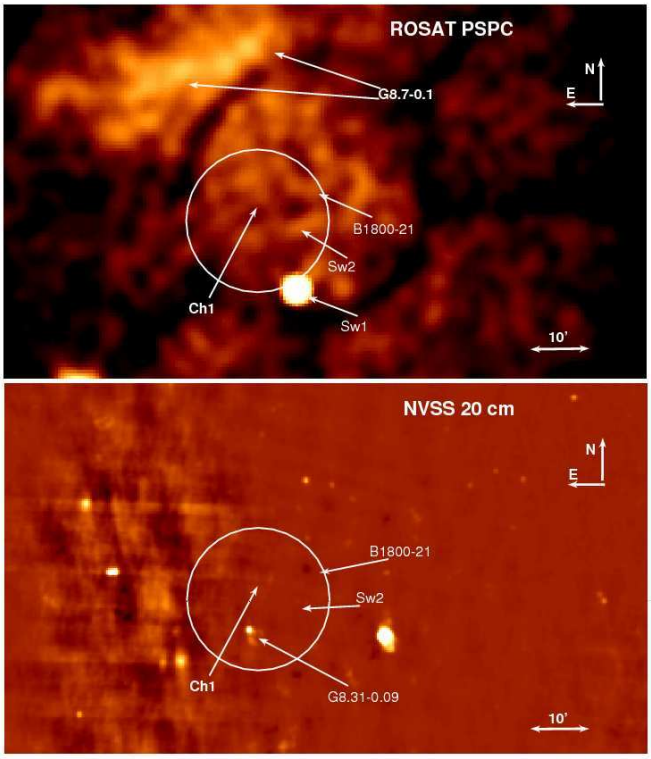

FIG. 8.— *Top:* 10 ks *ROSAT* PSPC image of the HESS J1804 field. The white circle ($r = 12'$) is centered at the best-fit position of HESS J1804. The diameter of the circle roughly corresponds to the extent of the γ-ray emission (see Ah06) The positions of the other sources discussed in the text are also marked. The brightest source Sw1 (=1RXS J180404.6– 215325) is most likely a nearby star DENIS J180403.2–215336 with magnitudes R = 12.0, J = 10.1, and K_s = 9.1. Sw2 (= 1WGA 1804.0–2142) corresponds to the bright source at the very bottom of the ACIS-S3 chip in Fig. 1; it positionally coincides with the other bright star, DENIS J180400.6–214252 (R = 13.9, J = 11.3, K = 10.15). *Bottom:* NVSS λ = 20 cm image of the same size (beam FWHM=45″). The only bright source within the circle is the G8.31–0.09 SNR candidate. The much fainter NVSS J180434–214025 (see §2.4) is not discernible in this image.

$B = 21$. However, since the interstellar extinction towards the inner Galactic buldge is very large ($A_V \simeq 18$ in the direction of Ch1 [$l = 8.^\circ429$, $b = -0.^\circ018$]; Schultheis et al. 1999), the limits are not very restrictive. We also examined the publically available data from the *Spitzer* GLIMPSE-II survey[5] covering the vicinity of HESS J1804 (see the 8 μm IRAC image in Fig. 7, *top*) but found no IR sources within 10″ from the Ch1 position, down to limiting fluxes of 5 and 6 μJy at 4.5 and 8 μm, respectively.

The closest match to Ch1 in radio catalogs was found in the NRAO VLA Sky Survey (NVSS) catalog (Condon et al. 1998). The catalog position of the relatively faint (27.6 ± 3.8 mJy) radio source, NVSS J180434–214025, is offset by 32″ from the Ch1 position, less than the NVSS beam size (45″ FWHM). However, the apparently extended NVSS source (linear size $\sim 1.'5$) looks like a part of a larger ($\sim 4'$ in diameter) diffuse structure, barely discernible in the NVSS image. Since the image of NVSS J180434–214025 shows some artificial structures, we cannot consider it as a true radio counterpart of Ch1 until it is confirmed by deeper observations.

The optical/NIR source nearest to Ch2 is located $\sim 28''$ away from the best-fit X-ray centroid (see Fig. 7). Having the magnitudes B = 14.54, V = 13.30, R = 12.19, J = 8.64, H = 8.05, and K = 7.67, and the proper motion of ≈ 10.6 mas yr^{-1} (NOMAD1 0682–0650954; Zacharias et al. 2005), it is likely a late-type M dwarf located at $d \approx 10$ pc. Such a dwarf could provide an X-ray flux of $\sim 10^{-13}$–10^{-12} ergs cm^{-2} s^{-1} (see, e.g., Hünsch et al. 1999; Preibisch et al. 2005), similar to those observed from Ch2/Su42. However, given its large offset from the brightest part of Ch2 (Fig. 2), the dwarf cannot account for the entire extended X-ray emission, although its flare might be responsible for the possible difference between the fluxes measured with *Suzaku* and *Chandra* (§2.2).

Ch3 is positionally coincident with the optical-NIR source DENIS J180421.4–214233, with magnitudes K = 11.9, H = 12.3, J = 13.3, I = 15.5, R = 16.8, V = 17.5, and B = 19.0, which is also seen in the 4.5 and 8 μm IRAC images. Within the X-ray extent of Ch4, there are five relatively bright 2MASS and DENIS sources (H magnitudes ranging from 10 to 14). Two IR sources within the X-ray extent of Ch4 are clearly seen in the IRAC images. One of them (northeast of the X-ray centroid of Ch4) is positionally coincident with the DENIS source J180423.6–213928 (J = 12.7, H = 10.0, and K = 8.8). The other IR source has a NIR counterpart NOMAD1 0683–0642056 (V = 17.2, J = 15.4, H = 11.7, and K = 10.0), with the proper motion of 208 mas yr^{-1}.

All the stars we found within the X-ray extents of Ch3 and Ch4 exhibit extremely red colors. Explaining such colors solely by extinction would require a very large absorbing column that would absorb any soft X-rays ($\lesssim 2$ keV) from this direction, in contradiction with the fact that we do see such X-rays from Ch3 and Ch4. The extremely red colors can be naturally explained if the NIR/IR objects are young pre-main-sequence (T Tauri) stars surrounded by dusty disks or infalling envelopes (e.g., Hartman et al. 2005). Indeed, the IRAC images show that the Ch3 and Ch4 regions are immersed in the extended diffuse IR emission (see Fig. 7) that may be associated with a nearby starforming region. The large proper motion of NOMAD1 0683–0642056 suggests a small distance to this star, $d \approx 100\,(v_\perp/100\,\mathrm{km\,s^{-1}})$ pc. Since the colors of this star are similar to those of the other stars around, it is likely that most of them belong to the same group, which is, perhaps, one of the nearest regions of star formation. Although the nearby T Tauri stars can easily account for the observed X-ray fluxes from Ch3 and Ch4 (e.g., Preibisch et al. 2005), such stars cannot produce TeV emission and, therefore, Ch3 and Ch4 are not associated with HESS J1804.

The IRAC images of the field (e.g., Fig. 7, *top*) reveal a large-scale diffuse emission with complex morphology. However, the IR brightness distribution does not correlate with the TeV brightness (shown by the contours in the same figure), nor with the large-scale X-ray brightness distribution seen in the archival *ROSAT* PSPC image (Fig. 8, *top*). The recently discovered radio source G8.31–0.09 (see the NVSS image in Fig. 8, *bottom*), classified as a possible SNR (Brogan et al. 2006), coincides well with the shell-like structure seen in the IRAC images (Fig. 7, *top*), thus confirming that the source is indeed a new SNR with an interesting IR morphology.

3. DISCUSSION.

We see from the *Chandra* ACIS image (Fig. 1) that the X-ray sky in the region of HESS J1804 is rich with point sources with fluxes of $\sim 10^{-14}$–10^{-13} erg cm^{-2} s^{-1}, most of which are possibly stars. Therefore, it is not surprising to find a few sources located relatively close to each other in this region of the sky. However, Ch1 does not have a known IR/optical counterpart while Ch2 appears to be extended, and both of them are located within the brightest part of HESS J1804 (1.′9

[5] http://www.astro.wisc.edu/sirtf/glimpsedata.html

and 2.′5 from the best-fit TeV position). This raises a possibility that at least one them is associated with the TeV source. Below we discuss whether Ch1 or Ch2 could be X-ray counterparts of HESS 1804, for several possible interpretations of the TeV source. Since the large extent of the TeV emission rules out association with extragalactic sources, we limit our consideration to the Galactic sources only.

3.1. *A High Mass X-ray Binary?*

As there are several HMXBs among the identified TeV sources (see examples in Table 2), we can consider the possibility that HESS J1804 is an HMXB and therefore may have a compact X-ray counterpart, such as Ch1 or Ch2. It is believed that in HMXBs particles can be accelerated up to ~ 10 TeV or even higher energies either in jets produced as the result of accretion onto a compact object (e.g., Bosch-Ramon 2006 and references therein) or in the pulsar wind, if the compact object is an active pulsar (e.g., Dubus 2006). Examples of such systems are the famous HMXB with the young PSR B1259–63 and the microquasars LS 5039 and LS I+61°303, for which the nature of the central engine (NS or BH) is still under debate. So far these are the only HMXB firmly detected in both the TeV and GeV bands. The ultra-relativistic particles can produce TeV emission via the inverse Compton scattering (ICS) of the optical-UV photons emitted by the non-degenerate companion or through the synchrotron self-Compton (SSC) process.

HMXBs produce X-rays either in the course of accretion of the matter from the secondary companion onto the compact object or via the synchrotron radiation in the shocked pulsar wind. We see from Table 2 that the TeV-to-X-ray (1–10 TeV to 1–10 keV) flux ratio, $f_\gamma/f_{\rm X}$, is $\lesssim 1$ for all the four HMXBs with more or less secure TeV associations, much smaller than $f_\gamma/f_{\rm X} \sim 30$ and 50 for Ch1 and Ch2, respectively. However, given the small size of the HMXB sample in Table 2 and the fact that $f_\gamma/f_{\rm X}$ varies by at least a factor of 10 within the sample, it is possible that some HMXBs have a higher $f_\gamma/f_{\rm X}$. Indeed, most of accreting binaries are strongly variable X-ray sources, some of them being X-ray transients. For instance, IGR J16358–4726, which is likely associated with HESS 1634–472 (Ah06), is a strongly variable X-ray source, with the 2–10 keV flux varying by a factor of $\gtrsim 4000$ (Patel et al. 2004; Mereghetti et al. 2006). This example demonstrates that the $f_\gamma/f_{\rm X}$ ratio in HMXBs may vary dramatically, especially in the cases when the TeV and X-ray fluxes are not measured simultaneously. Thus, the rather modest X-ray luminosities of Ch1 and Ch2 could be explained assuming that either of them is an HMXB in the low/hard state.

The hard ($\Gamma \sim 0.5$) X-ray spectrum of Ch1 is strongly absorbed; the hydrogen column density, $n_{\rm H,22} \simeq 4$, is a factor of 2–3 larger than the total Galactic HI column ($\simeq 1.5\times10^{22}$ cm^{-2}; Dickey & Lockman 1990) and a factor of 2–4 larger than the $n_{\rm H,22} \sim 1.4$ inferred from the X-ray spectrum of PSR B1800–21 (and its PWN) located at the distance of ≈ 4 kpc (Kargaltsev et al. 2006a). Taking into account that the $n_{\rm H}$ value deduced from an X-ray spectrum under the assumption of standard element abundances generally exceeds the $n_{\rm HI}$ measured from 21 cm observations by a factor of 1.5–3 (e.g., Baumgartner & Mushotzky 2005), the large $n_{\rm H}$ (consistent with $A_V \sim 20$; e.g., Predehl & Schmitt 1995) suggests that Ch1 is either located within (or even beyond) the Galactic Buldge or it shows intrinsic absorption, often seen in X-ray spectra of HMXBs (e.g., Walter et al. 2006).

As the spin periods of NSs in HMXBs range from a fraction of second to thousands of seconds, the HMXB interpretation provides a plausible explanation for the putative 106 s periodicity in Ch1, which would be difficult to interpret otherwise. On the other hand, the lack of an IR/NIR counterpart is somewhat surprising, although the upper limits on the unabsorbed IR/NIR fluxes (see §2.4 and Fig. 9) still cannot rule out a B-giant at a distance of $\gtrsim 8$ kpc.

We found no *CGRO* EGRET counterparts for Ch1 and other sources in the HESS J1804 field. The nearest EGRET source (Hartman et al. 1999) is located $\simeq 2.^\circ2$ from the Ch1 position, too far to be associated with HESS J1804 or the *Chandra* sources. However, only three HMXBs (PSR B1259–63, LS 5039 and LS I+61°303) have been identified with EGRET sources so far. The upper limit on GeV flux, obtained from the EGRET upper limits map (Fig. 3 from Hartman et al. 1999), is not deep enough to test the connection between the X-ray spectrum of Ch1 and the TeV spectrum of HESS J1804 (see Fig. 9). The *Intergal* ISGRI upper limit (A. Bykov 2006, priv. comm.), shown in the same figure, appears to be even less restrictive. From Figure 9 we can only conclude that the TeV spectrum of HESS J1804 breaks somewhere between the EGRET and HESS energy ranges, as observed for many TeV sources of different kinds.

The spectral parameters of the Ch2 source are very uncertain. Although the flux measured with *Chandra* is somewhat lower than that measured with *Suzaku* a year later (see §2.2), the difference is only marginal because of the large uncertainties of the measurements. However, if confirmed, the variability would be an argument supporting an HMXB interpretation of Ch2. On the contrary, the rather large X-ray extent of Ch2 [$\sim 1' = 2(d/7\,{\rm kpc})$ pc] argues against the X-ray binary interpretation[6]. Although possible X-ray emission from a nearby M-dwarf (§2.4) may contribute to Ch2, it cannot account for the entire emission from this extended or multiple source.

Even if either of the X-ray sources is an HMXB, a major problem with its association with HESS J1804 is the extended morphology of the latter. Although, there is no an *a priori* reason to believe that HMXBs cannot produce extended TeV emission, the observational evidence for that is currently rather weak. So far, among the TeV sources possibly associated with HMXBs, only two, HESS J1632–478 and HESS J1634–472, might show extended TeV emission (Ah06), and the evidence for the extension is marginal in both cases.

Thus, although an HMXB at a distance of ~ 8–15 kpc remains a plausible interpretation for Ch1[7] and somewhat less plausible for Ch2, the association between them and the TeV source is very questionable. An HMXB origin of Ch1 or Ch2 would be firmly established if the periodic (and/or non-periodic) variability is confirmed for Ch1 (or found for Ch2) in a deeper X-ray observation, or a companion star is detected in the IR-optical. At the same time, a deeper on-axis observation with *Chandra* can measure the true extent and spatial structure of Ch2.

[6] To our knowledge, extended X-ray emission has been reported only from three HMXBs: SS 433 (Migliari, Fender, & Méndez 2002), Cyg X-3 (Heindl et al. 2003), and XTE J1550–564 (Corbel et al. 2002). This emission is often attributed to jets. In these systems the angular extent of the resolved X-ray emission ranges from 3″ to 30″ corresponding to physical lengths of 0.1 to 0.8 pc at the nominal distances to these systems. No TeV emission has been reported from these HMXBs yet.

[7] We should mention that, based on the strongly absorbed, hard X-ray spectrum, this source can also be a background AGN.

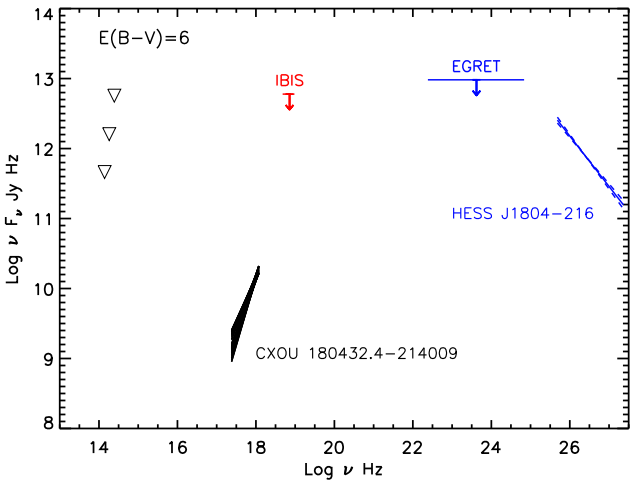

FIG. 9.— Unabsorbed spectra of Ch1 and HESS J1804 (Ah06), together with the *CGRO* EGRET and *INTEGRAL* IBIS/ISGRI upper limits. The open triangles show the upper limits on the dereddened NIR fluxes in the K_s, H, and J bands (see §2.4).

3.2. *A Pulsar Wind Nebula?*

Among other types of Galactic X-ray sources, only SNR shocks and PWNe are believed to be able to produce extended TeV emission. In fact, the second highest (persistent) TeV-to-X-ray flux ratio, $f_\gamma/f_X = 3.4$, in Table 2 belongs to the PWN G18.0–0.7 around the Vela-like pulsar B1823–13 ($\dot{E} \approx 3\times10^{36}$ erg s^{-1}; $d \approx 4$ kpc), likely associated with HESS J1825–137 (Ah06). Although no SNR has been associated with this pulsar, it powers a luminous extended X-ray PWN ($L_X \sim 3\times10^{33}$ erg s^{-1}, angular size $\gtrsim 5'$; Gaensler et al. 2003). In addition to the extended low-surface-brightness component, G18.0–0.7 has a much more compact (5″–10″) brighter core, resolved by *Chandra* (Teter et al. 2004; Kargaltsev et al. 2006b). The TeV emission detected with HESS covers a much larger area than the X-ray emission from G18.0–0.7, extending up to 1° southward from the pulsar (Aharonian et al. 2006c). However, both the TeV and the low-surface-brightness X-ray emission have similarly asymmetric shapes, and they are offset in the same direction with respect to the pulsar position. A similar picture is observed around the Vela pulsar ($\dot{E} \approx 7\times10^{36}$ erg s^{-1}; $d \approx 300$ pc). An X-ray bright, compact ($\sim 40''$ in diameter) PWN centered on the pulsar is accompanied by a much larger ($\sim 50'$) but dimmer asymmetric diffuse X-ray component (sometimes referred to as "Vela X"), which also has a TeV counterpart (Aharonian et al. 2006d).

The asymmetry in the extended PWN components can be caused by the reverse SNR shock that had propagated through the inhomogeneous SNR interior towards the SNR center and reached one side of the PWN sooner than the other side (e.g., Blondin, Chevalier, & Frierson 2001). The wind, produced by the pulsar over a substantial period of time (up to a few kyrs) and therefore occupying a substantial volume, could be swept up by the reverse shock wave into a smaller volume on one side of the PWN. The swept-up wind confined within the formed "sack" emits synchrotron radiation in X-rays. At the same time, the wind can produce TeV radiation via the ICS of the cosmic microwave background (CMB) and synchrotron photons off the relativistic electrons[8]. The Lorentz factor of the electron that upscatters the CMB photon to the energy $\mathcal{E}_\gamma$ is $\gamma \approx 10^8(\mathcal{E}_\gamma/9\ \mathrm{TeV})^{1/2}$. Electrons with such Lorentz factors emit synchrotron photons with energies $\mathcal{E}_{\rm syn} \sim 0.5\gamma_8^2(B/10\ \mu\mathrm{G})\mathrm{keV} \sim 0.5(\mathcal{E}_\gamma/9\ \mathrm{TeV})(B/10\ \mu\mathrm{G})$ keV. Therefore, the observed TeV spectrum of HESS J1804, spanning from 0.2 to 10 TeV (Ah06), would correspond to the $\approx$ 0.01–0.6 keV range of the synchrotron photon energies in $B = 10\ \mu$G. These EUV and soft X-ray synchrotron photons are heavily absorbed at $n_{\rm H} \gtrsim 10^{22}$ cm^{-2} and hence are difficult to detect. Thus, if the swept-up wind is cold enough [e.g., $\gamma \lesssim 10^8(B/10\,\mu\mathrm{G})^{-1/2}$], the sack may be bright in TeV but faint in the *Chandra* band. Furthermore, the magnetic field inside the sack is lower than that in the compact PWN, leading to a lower synchrotron brightness since the latter depends on the magnetic field strengths as $B^{(p+1)/2}$ for the PL distribution of electrons, $dn_e = K\gamma^{-p}d\gamma$. This could explain why the TeV emitting region is dimmer in X-rays than the compact PWN populated with more energetic electrons, but it does not explain why the compact PWN shows lower surface brightness in TeV than the extended asymmetric PWN. The brightness of the TeV emission produced via the ICS on CMB photons does not depend on the magnetic field; therefore, the simplest explanation could be that the sack contains a larger number (and perhaps a higher column density) of the swept-up TeV-emitting electrons compared to those within the compact PWN.

One could try to apply the above interpretation to HESS J1804, assuming that Ch1 (or Ch2) is a pulsar with a PWN. The off-axis position may not allow one to resolve a compact PWN. Furthermore, Bamba et al. (2006) report Su40 (=Ch1) as an extended source, which could mean that the more sensitive (on large angular scales) *Suzaku* XIS observation has detected a fainter extended PWN component (similar to the *XMM-Newton* observation of B1823–13; Gaensler et al. 2003). The faintness of a possible extended PWN component could be at least partly attributed to the strong X-ray absorption in this direction. On the other hand, Ch2 is resolved by *Chandra* into an extended X-ray source, which might be a PWN. However, the low S/N and the off-axis location hamper the assessment of the spatial structure and the spectrum of Ch2.

The 3.24 s time resolution of the ACIS observation also precludes a search for sub-second pulsations expected from a young pulsar (the putative 106 s period of Ch1 is certainly too long for a young isolated pulsar and hence should be attributed to a statistical fluctuation in this interpretation). Keeping in mind the above examples of Vela X and G18.0–0.7, the large extent of HESS J1804 should not be alarming. A lack of strong asymmetry with respect to the pulsar, which is the distinctive feature of all the other extended TeV PWNe (Table 2; de Jager 2006), could be attributed to the low sensitivity of the *Chandra* observation to extended emission of low surface brightness or to the projection effect (i.e., the TeV PWN could be displaced from the pulsar along the line of sight). The large f_γ/f_X values cast additional doubts on the PWN interpretation; however, even a luminous extended X-ray component of low surface brightness could remain undetected in the relatively shallow off-axis ACIS exposure. A

[8] An alternative TeV production mechanism is $\pi^0 \rightarrow \gamma+\gamma$ decay, with π^0 being produced when the relativistic protons of the pulsar wind interact with the ambient matter (Horns 2006). Although the presence of the hadronic component in the pulsar wind has not yet been established observationally, it is expected to be present according to some pulsar wind acceleration models (e.g., Arons 2005).

deeper on-axis observation with *Chandra* would test the nature of Ch1 and Ch2 and the PWN interpretation. Overall, although not excluded, the possibility that Ch1 or Ch2 are the pulsars powering the TeV PWN does not look very compelling at this point.

On the other hand, the association of HESS J1804 with the Vela-like pulsar B1800–21 remains a plausible option. To date, young Vela-like pulsars have been found in the vicinity of ~ 10 extended TeV sources (e.g., de Jager 2006; Gallant 2006). Since both pulsars and TeV sources are concentrated in the Galactic plane, and the extended TeV sources have typical sizes of $\sim 5' - 15'$, one could attempt to explain this by a chance coincidence. However, the probability of chance coincidence is low. For instance, within the $\simeq 300$ square degrees area of the Galactic plane, surveyed by HESS (Ah06) the surface density of young (≤ 100 kyrs) pulsars is ≈ 0.13 deg^{-2} (based on the ATNF Pulsar Catalog data; Manchester et al. 2005). On the other hand, the same area includes four extended TeV sources (HESS J1825–137, HESS J1809–193, HESS J1804–216, and HESS J1616–508) located within $15'$ from one of the young pulsars. Since the probability of finding a young pulsar within an arbitrary placed R= $15'$ circle is only 2.6%, the probability of accidentally having all the four TeV sources within the $15'$ distances from the young pulsars is negligible, $0.026^4 \approx 5 \times 10^{-7}$. This strongly suggests a physical connection between the two phenomena (e.g., de Jager 2006). Furthermore, there are several pairs, such as PSR B0833–45/HESS J0835–455, PSR B1509–58/HESS J1514–591, and PSR B1823–13/HESS J1825–137, for which the connection is supported by the correlation between the TeV and X-ray brightness distributions. Note, that in these pairs the pulsars are offset by $10'$–$15'$ from the peaks of the TeV brightness.

From the theoretical perspective, the "crushed PWN" hypothesis (Blondin et al. 2001), briefly discussed above, provides a possible explanation for the observed offsets. From the observational point of view, the associations are supported by the detection of large, asymmetric X-ray structures correlated with the TeV brightness distributions and apparently connected to the pulsars. However, in several possible associations the existing X-ray images are not deep enough to reveal an extended PWN component. In particular, the X-ray images of the PWN around B1800–21 (Kargaltsev et al. 2006a) show a hint of a dim, asymmetric PWN component extended toward HESS J1804, but the sensitivity of the *Chandra* observation was possibly insufficient to detect the PWN beyond $15''$–$20''$ from the pulsar. This is similar to PSR B1823–13, where the arcminute-scale PWN was well seen only in a long *XMM-Newton* observation, and only *a posteriori* a hint of it was found in the *Chandra* data (Kargaltsev et al. 2006b). Hence, there is a good chance that PSR B1800–21 also has a dim, asymmetric PWN. It could be detected in a deep *XMM-Newton* exposure, thereby establishing the association between HESS J1804 and PSR B1800–21.

3.3. *An SNR shock?*

While discussing the Su40 (=Ch1) and Su42 (=Ch2) association with HESS J1804, Bamba et al. (2006) suggest that the X-ray and TeV emission could come from an SNR shock (possibly in G8.7–0.1). In our opinion, the fact that the angular extent of the two X-ray sources is much smaller than the extent of the TeV emission (see Fig. 1) is a strong argument against such an interpretation[9]. Nevertheless, a possibility that an SNR (so far undetected in X-rays) could produce the observed TeV emission in HESS J1804 (see Fatuzzo, Melia, & Crocker 2006) cannot be ruled out if the TeV source is not associated with Ch1, Ch2, or PSR B1800–21.

Indeed, contrary to the conclusion by Bamba et al. (2006)[10], the close match in the sky positions of Ch1 (or Ch2) and HESS J1804 can merely be a chance coincidence, and HESS J1804 may have no point-like X-ray counterparts down to the 3σ limiting flux of $\lesssim 1 \times 10^{-14}$ ergs s^{-1} cm^{-2} within the TeV bright region. However, one cannot exclude the presence of faint diffuse X-ray emission, e.g. from an SNR whose image size exceeds the chip size. Since it is difficult to estimate which fraction of the observed diffuse count rate (1.3 counts ks^{-1} arcmin^{-2} in the I3 chip; see §2.1) comes from the background and what is the nature of the remaining flux (e.g., thermal emission from an SNR or nonthermal emission from an extended PWN), we can only put an upper limit of 2.5×10^{-12} ergs s^{-1} cm^{-2} on the 2–10 keV flux in the I3 chip area, corresponding to $f_\gamma / f_X \gtrsim 4$ (this estimate assumes $n_{H,22} = 1$ and a PL model with $\Gamma = 1.5$). However, we do not see any significant large-scale (in comparison with the off-axis PSF size) X-ray brightness variations in the ACIS image. (see Figs. 1 and 2). Although such uniformity is somewhat unusual for an SNR, we note that the interior of the shell-type SNR RX J1713.7–3946 (resolved into a $\approx 1^\circ$ shell in TeV; Aharonian et al. 2004) is relatively faint and homogeneous in X-rays (Hiraga et al. 2005). Furthermore, following Kargaltsev et al. (2006a), we conclude that if the X-ray spectrum and luminosity of the undetected SNR are similar to those of the Vela SNR, the expected off-axis ACIS-I3 surface brightness is < 0.3 counts ks^{-1} arcmin^{-2} in the 0.5–7 keV band (for the Raymond-Smith thermal plasma emission models with $T < 3$ MK and $n_{H,22} = 1$), i.e. at least a factor of 4 below the observed upper limit (see §2.1.1).

On the other hand, the TeV brightness distribution in HESS J1804 poorly correlates with the radio brightness distribution. Although located within the boundaries of G8.7–0.1, the region around HESS J1804 in the radio image is much dimmer than the northeast part of G8.7–0.1 that also emits X-rays observed with *ROSAT* (see Fig. 8). This, in our view, argues against the HESS J1804 and G8.7–0.1 association (see, however, Fatuzzo et al. 2006, who argue that the TeV emission can be produces by a shock in the G8.7–0.1 interacting with a molecular cloud).

A possibility that HESS J1804 is associated with the recently discovered faint radio (and IR) source G8.31–0.09, likely an SNR (Brogan et al. 2006), is not attractive either. G8.31–0.09 is outside the ACIS FOV, and it is not seen in the archival *ROSAT* PSPC image (Fig. 8; *top*). However, G8.31–0.09 is far from the peak of the TeV brightness distribution (see the *Spitzer* image in Fig. 7). Furthermore, the size of the shell-like G8.31–0.09 in the *Spitzer* image is much smaller than the TeV extent of HESS J1804 and hence, even if G8.31–0.09 is indeed an SNR, it is unlikely to be related to

[9] For instance, the RX J1713.7–3946 and G266.6-1.2 SNRs have comparable sizes in X-rays and TeV.

[10] These authors state that the expected number of sources within the area defined by the error bars of the HESS J1804 best-fit position should be very small, $(4-9) \times 10^{-3}$. First, one should not use the uncertainty of the best-fit TeV position for such an estimate when the TeV source is clearly extended and asymmetric. Second, as we see from Fig. 1, the probability of finding an X-ray source with a flux of 10^{-14}–10^{-13} ergs s^{-1} cm^{-2} within an arbitrary placed $r = 1'$ circle is quite high.

HESS J1804.

4. SUMMARY

We serendipitously detected several X-ray sources, whose positions are close to the maximum of the TeV brightness distribution of the extended VHE source HESS J1804. Among these sources, only Ch1 and Ch2 might be related to HESS J1804. The fact that HESS J1804 is an extended source rules out an extragalactic (i.e. AGN) origin, and it also argues against an HMXB interpretation.

On the other hand, the marginal detection of 106 s pulsations in Ch1 suggests that Ch1 might be an HMXB unrelated to HESS J1804. There also remains a possibility that Ch1 is a new obscured pulsar/PWN couple, possibly associated with G8.7−0.1. In this case no variability is expected on time scales $\gtrsim 1$ s, but one could expect to see an X-ray PWN, which has not been detected in the *Chandra* observation possibly because of the off-axis placement on the ACIS detector.

A possible variability of Ch2 on a year timescale might also suggest that Ch2 is an accreting binary, which makes the association with HESS J1804 unlikely. On the other hand, the extended appearance of Ch2 argues in favor of a PWN or a remote SNR. In the former case, there remains a possibility of association of Ch2 with HESS J1804. Further on-axis observations with *Chandra* ACIS are needed to firmly establish the nature of the two sources.

It is possible that neither Ch1 nor Ch2 are associated with HESS J1804. In this case the most plausible interpretation of HESS J1804 is that the TeV emission comes from an X-ray dim part of the asymmetric PWN created by PSR B1800–21. A longer observation with *XMM-Newton* or *Chandra*, combined with deep high-resolution imaging in the radio and IR, will finally differentiate between these possibilities and establish the nature the two *Chandra* sources as well as the origin of the TeV emission.

Our thanks are due to Andrey Bykov for providing the *Integral* IBIS/ISGRI upper limit for the HESS J1804 flux. We are also grateful to Konstantin Getman for the useful discussions about multiwavelength emission from young stars. This work was partially supported by by NASA grants NAG5-10865 and NAS8-01128 and *Chandra* awards AR5-606X and SV4-74018.

REFERENCES

Aharonian, F. et al. 2004, Nature, 432, 75
Aharonian, F. et al. 2005a, Science, 307, 1938
Aharonian, F. et al. 2005b, A&A, 442, 1
Aharonian, F. et al. 2005c, A&A, 437, 95
Aharonian, F. et al. 2005d, A&A, 437, 7
Aharonian, F. et al. 2005e, A&A, 435, 17
Aharonian, F. et al. 2005f, A&A, 432, 25
Aharonian, F., et al. 2006a, ApJ, 636, 777 (Ah06)
Aharonian, F., et al. 2006b, A&A, accepted (astro-ph/0607192)
Aharonian, F., et al. 2006c, A&A, accepted (astro-ph/0607548)
Aharonian, F., et al. 2006d, A&A, 448, 43
Aharonian, F., et al. 2006e, A&A, 460, 743
Aharonian, F., et al. 2006f, A&A, 449, 223
Aharonian, F., et al. 2006g, A&A, 457, 899
Albert, J., et al. 2006a, Science, 312, 1771
Albert, J., et al. 2006b, ApJ, 642, 119
Arons, J. 2004, Adv. Space Res. 33, 466
Bamba, A., et al. 2006, PASJ, in press (astro-ph/0608310)
Baumgartner, W. H., & Mushotzki, R. F. 2006, ApJ, 639, 929
Blondin. J., Chevalier, R., & Frierson, D. 2001, ApJ, 563, 806
Bosch-Ramon, V., et al. 2005, ApJ, 628, 388
Bosch-Ramon, V. 2006, Astrophys. Space Sci, in press (astro-ph/0612318)
Brogan, C. L., Gelfand, J. D., Gaensler, B. M., Kassim, N. E., & Lazio, T. J. 2006, ApJ, 639, L25
Chernyakova, M., Neronov, A., Lutovinov, A., Rodriguez, J., & Johnston, S. 2006, MNRAS, 367, 1201
Condon, J. J., Cotton, W. D., Greisen, E. W., Yin, Q. F., Perley, R. A., Taylor, G. B., & Broderick, J. J. 1998, AJ, 115, 1693
Corbel, S., Fender, R. P., Tzioumis, A. K., Tomsick, J. A., Orosz, J. A., Miller, J. M., Wijnands, R., & Kaaret, P. 2002, Science, 298, 196
Cui, W., & Konopelko, A. 2006, ApJ, 625, L109
Cutri, R. M., et al. 2003, 2MASS All-Sky Catalog of Point Sources, VizieR On-line Data Catalog: II/246
de Jager, O. 2006, On the Present and Future of Pulsar Astronomy, 26-th meeting of IAU, Joint Discussion 2, 16-17 August, 2006, Prague, Czech Republic, JD02, #53
Dickey, J. M., & Lockman. F. J. 1990, ARA&A, 28, 215
Dubus, G. 2006, A&A, 456, 801
Finley, J. P., & Ögelman, H. 1994, ApJ, 434, L25
Fatuzzo, M., Melia, F., & Crocker, R. M. 2006, ApJ, accepted (astro-ph/0602330)
Gaensler, B. M., Pivovaroff, M. J., & Garmire, G. P. 2001, ApJ, 556, 107
Gaensler, B. M., et al. 2002, ApJ, 569, 878
Gaensler, B. M., et al. 2003, ApJ, 588, 441
Gallant, Y. 2006, to appear in Proc. "The Multi-Messenger Approach to High-Energy Gamma-Ray Sources", Barcelona, July 2006 (astro-ph/0611720)
Hartman, R. C., et al. 1999, ApJS, 123, 79
Hartmann, L., et al. 2005, ApJ, 629, 881
Harrison, F. A., et al. 2000, ApJ, 528, 454
Heindl, W. A., Tomsick, J. A., Wijnands, R., & Smith, D. M. 2003, ApJ, 588, L97
Hiraga, J. S. 2005, A&A, 431, 953
Horns, D., et al. 2006, to appear in Proc. "The Multi-Messenger Approach to High-Energy Gamma-Ray Sources", Barcelona, July 2006 (astro-ph/0609386)
Hünsch, M., Schmitt, J. H. M. M., Sterzik, M. F., & Voges, W. 1999, A&A Supp., 135, 319
Iyudin, A. F., Aschenbach, B., Becker, W., Dennerl, K., & Haberl, F. 2005, A&A, 429, 225
Kargaltsev, O., Pavlov, G. G., & Garmire, G. P. 2006a, ApJ, submitted (astro-ph/0611599)
Kargaltsev, O., Pavlov, G. G., Sanwal, D., Wong, J., & Garmire G. P. 2006b, AAS HEAD meeting 9, #7.57
Landi, R., et al. 2006, ApJ, 651, 190
Lutovinov, A., et al. 2005, A&A, 444, 821
Manchester, R. N., Hobbs, G. B., Teoh, A., & Hobbs, M. 2005, AJ, 129,1993
Markwardt, C. B., & Ögelman, H. B. 1997, ApJ, 480, 13
Mereghetti, S., et al. 2006, A&A, 450, 759
Migliari, S., Fender, R. P., & Méndez, M. 2002, Science, 297, 1673
Ong, R. A. 2006, Rapporteur Talk at 29th International Cosmic Ray Conference in Pune, India, 2005 (astro-ph/0605191)
Patel, S. K., et al. 2004, ApJ, 602, 45
Predehl, P., & Schmitt, J. H. M. M. 1995, A&A, 293, 889
Preibisch, T., et al. 2005, ApJS, 160, 401
Teter, M. A., Sanwal, D., Pavlov, G. G., & Tsuruta, S. 2003, BAAS, 35, 706
Schultheis, M., et al. 1999, 349, L69
Walter, R., et al. 2006, A&A, 453, 133
Zacharias, N., et al. 2005, VizieR On-line Data Catalog: I/297
Zavlin, V. E., Pavlov, G. G., Sanwal, D., & Trümper, J. 2000, ApJ, 540, 25

TABLE 2
X-RAY AND TEV PROPERTIES FOR DIFFERENT TYPES OF OBJECTS DETECTED AT $E > 1$ TEV.

Name	Type	f_X [a]	Γ_X	f_γ [b]	Γ_γ	f_γ/f_X	Extended in TeV?	Variability	X-ray counterpart	Ref.[c]
LSI +61 303	HMXB/μ-quasar	0.64	1.8	0.54	2.6	0.8	no	$P_{\rm orb}$ = 26 d	yes	1,2
LS 5039	HMXB/μ-quasar	0.90	1.6	0.62	2.1	0.7	no	$P_{\rm orb}$ = 4.4 d	yes	3,4
PSR B1259–63	HMXB/pulsar	0.6	1.4	0.24	2.7	0.4	no	$P_{\rm spin}$ = 48 ms, $P_{\rm orb}$ = 3.4 yrs	yes	5,6
HESS J1634–472	HMXB/NS?	0.004–16.5	0.5	0.50	2.4	0.03–125	yes?	P = 5890 s , X-ray transient	IGR J16358–4726?	7,8
HESS J1632–478	HMXB?	8.8	0.7	1.7	2.1	0.2	yes?	$P_{\rm spin}$ = 1300 s, $P_{\rm orb}$ = 9 days	IGR J16320–4751	7,9,10
1ES 1218+30.4	BL Lac	2.4	1.4	0.73	3.0	0.3	no	yes	yes	11
Mkn 421	BL Lac	24.9	1.5	49.3	2.1	2.0	no	yes	yes	12
RX J1713.7–3946	SNR	80	2.3	6	2.2	0.075	yes	no	G347.3–0.5	13,14
G266.6–1.2	SNR	11.8	2.6	7	2.1	0.6	yes	no	Vela Junior	15, 16
Crab	PWN	868	2.1	6.7	2.6	0.008	no	no	Crab PWN	17
HESS J1825–137	PWN	0.14	2.3	0.48	2.4	3.4	yes	no	B1823–13 PWN	18, 19
MSH 15–52	PWN	5.5	1.9	1.5	2.3	0.27	yes	no	yes	20, 21
Vela X	PWN	7.4	2.1	4.6	1.45	0.6	yes	no	yes	22, 23
G0.9+0.1	PWN?	1.6	2.3	0.19	2.4	0.1	no?	no	yes	24 25
HESS J1804/Ch1[d]	?	0.03	0.45	0.91	2.7	30	yes	$P_{\rm spin}$ = 106 s ?	yes	–
HESS J1804/Ch2[e]	?	0.02	?	0.91	2.7	50	yes	?	yes	–
HESS J1804/Diff.[f]	?	$\lesssim 0.25$	1.5	0.91	2.7	$\gtrsim 4$	yes	no	yes	–

[a]Unabsorbed X-ray flux (1–10 keV) in units of 10^{-11} ergs cm^{-2} s^{-1} obtained from the PL fit with the photon index Γ_X.
[b]Unabsorbed γ-ray flux (1–10 TeV) in units of 10^{-11} ergs cm^{-2} s^{-1} obtained from the PL fit with the photon index Γ_γ.
[c] References to the papers where the parameters listed in the table were measured.– (1) Albert et al. (2006a); (2) Harrison et al. (2000); (3) Aharonian et al. (2006e); (4) Bosch-Ramon et al. (2005); (5) Chernyakova et al. (2006); (6) Aharonian et al. (2005b); (7) Aharonian et al. (2006a); (8) Patel et al. (2004); (9) Lutovinov et al. (2005); (10) Walter et al. (2006); (11) Albert et al. (2006b); (12) Aharonian et al. (2005c); (13) Aharonian et al. (2006f); (14) Hiraga et al. (2005); (15) Aharonian et al. (2005d); (16) Iyudin et al. (2005); (17) Aharonian et al. (2006g); (18) Aharonian et al. (2006c); (19) Gaensler et al. (2003); (20) Aharonian et al. (2005e); (21) Gaensler et al. (2002); (22) Aharonian et al. (2006d); (23) Markwardt & Ogelman (1997); (24) Aharonian et al. (2005f); (25) Gaensler, Pivovaroff, & Garmire (2001)
[d]Assuming HESS J1804/Ch1 association.
[e]Assuming HESS J1804/Ch2 association.
[f]An upper limit on the X-ray flux corresponds to the diffuse background on the ACIS-I3 chip (see §3.3).